Coercivity mechanism of rare-earth free MnBi hard magnetic alloys

J. Zamora, I. Betancourt*, and I.A. Figueroa
Departamento de Materiales Metálicos y Cerámicos, Instituto de Investigaciones en Materiales, Universidad Nacional Autónoma de México, México D.F. 04510.
**e-mail: israelb@unam.mx*

Received 19 June 2017; accepted 3 January 2018

In this work, we present and discuss results concerning the hard magnetic behavior of rare earth-free MnBi alloys obtained by suction casting technique. The physics of coercivity for these type of alloys is based on the nucleation process of reverse domains, which in turn is determined by the alloy microstructure features such as phase distribution, morphology, grain size and in particular, defects, which are characteristic of real materials. The microstructure of the as-cast alloy presented here comprises the formation of the Low Temperature Intermetallic Phase (LTIP)-MnBi, interspersed within Bi- and Mn-rich areas. A considerable intrinsic coercivity field of 238 kA/m together with a saturation magnetization of 0.04 T were observed. The nucleation controlled mechanism of this alloy was described in terms of the Kronmüller equation, which incorporates the detrimental effect of microstructure defects through fitting parameters associated to reduced intrinsic magnetic properties at grain size boundaries, interfaces and local demagnetizing fields. A notorious switching of coercivity mechanism associated with domain wall pinning was found to be produced upon annealing of the alloy at 583 K for 24 hrs, yielding a drastic reduction of coercivity (down to 16 kA/m). The key microstructural feature determining the switching of coercivity mechanism is the formation/suppression of Bi-rich areas, which promotes the nucleation and growth of LTIP.

Keywords: Magnetic materials; hard magnetic properties; coercivity.

PACS: 75; 75.30.Gw; 75.50.Vv; 75.50.Ww

1. Introduction

MnBi-based alloys are considered an attractive alternative as precursor materials for designing permanent magnets due to the formation of the Low Temperature Intermetallic Phase (LTIP)-MnBi, which is a ferromagnetic phase with a NiAs-type hexagonal structure and spatial group $P6_3/mmc$. The uniaxial magnetocrystalline anisotropy of this phase possesses a magnetocrystalline anisotropy constant (K_1) as high as 0.90×10^6 J/m^3 together with a saturation magnetization ($\mu_0 M_s$) of 0.73 T [1-2] as well as a positive temperature coefficient of coercivity [3-6], which enables these alloys for potential applications in permanent magnets capable to operate at high temperatures [7]. An additional feature of these MnBi alloys is their rare-earth free content, which will represent a competitive advantage in terms of cost for production relative to the well established Nd-Fe-B alloys for supermagnets production. However, preparation of a single phase LTIP-MnBi alloy is not easy because its characteristic peritectic reaction, which promotes the formation of secondary phases [8-12].

In order to develop high coercivity magnets with optimum performance, the key issue from the theoretical point of view is the physical understanding of the coercivity mechanism driving the magnetic hardening of the material. There are two main theoretical approaches for describing the coercivity (H_c) of magnetic materials: nucleation controlled process and pinning of magnetic domain walls. For nucleation process, the development of high coercivities relies on the nucleation field H_N necessary for the onset of magnetization reversal taking place at the interface of non-magnetic grains, defects or significant misalignment between magnetic grains. According to Kronmüller [13,14], in order to incorporate the detrimental influence of microstructural defects in real materials (point defects, grain boundaries, non-magnetic phases) the proper equation for H_c is given by

$$H_c = H_N \alpha_K - N_{\text{eff}}(\mu_0 M_S) \tag{1}$$

Where H_N stands for the nucleation field (H_N=K_1/M_S), α_K is a microstructural parameter representing the reduction of K_1 at the surface interfaces with non-magnetic regions and N_{eff} is an average effective demagnetization factor describing the internal stray fields acting on the grains.

On the other hand, pinning of magnetic domain walls depends on the size and morphology of the phases present within the material's microstructure. The critical length L_{crit} for the formation of magnetic domains is given by [13]

$$L_{\text{crit}} = \frac{72}{\mu_0 M_S^2}\sqrt{AK_1} \tag{2}$$

Where A corresponds to the exchange constant of the material. If the magnetic phase has a characteristic length $L > L_{\text{crit}}$, magnetic domains will appear as part of the magnetic structure in order to decrease the magnetostatic energy of the material. The concomitant formation of magnetic domain walls will promote a coercivity mechanism by means of their pinning at the defects of the materials' microstructure, such as inclusions, secondary non-magnetic phases, vacancies, grain boundaries or interfaces, for which the intrinsic magnetic properties (such as K_1, A or M_s) are usually reduced or even vanished. For pinning mechanism, the propagation field H_p associated to the coercivity of the material can be calculated as follows [15]:

$$H_p = \frac{\gamma_w}{\mu_0 M_S R_0} \quad (3)$$

Where γ_w stands for the energy of the domain wall, and R_0 corresponds to the radius of the inclusion.

In this work, we discuss the phase constitution and its influence on the coercivity mechanism of MnBi alloys obtained by suction casting technique

2. Experimental Techniques

Master ingots of composition $Mn_{0.5}Bi_{0.5}$ were prepared by arc-melting technique of elemental constituents under Ar atmosphere. From the master ingots, cylindrical rods (3 mm diameter and 30 mm length) were obtained by suction casting technique. A subsequent annealing was applied for selected samples at 583 K for 24 h, followed by quenching process in water. Phase distribution and microstructural analysis was performed by means of Field Emission Scanning Electron Microscopy. Magnetic measurements were carried out at room temperature using a Vibrating Sample Magnetometer with maximum applied fields within the range 1500 - 2500 kA/m.

3. Results

Figure 1 shows a Scanning Electron Microscopy (SEM) micrograph for the as-cast MnBi alloy, for which three different regions are evident: Black zones dispersed over a dominant light gray region, together with dark gray areas. Energy Dispersive Spectroscopy (EDS) composition analysis showed that such regions correspond to pure Mn and Bi, and, the LTIP-MnBi respectively. LTIP is observed throughout the sample with undissolved Mn particles embedded in a diamagnetic Bi-rich matrix. According to the inset showing further

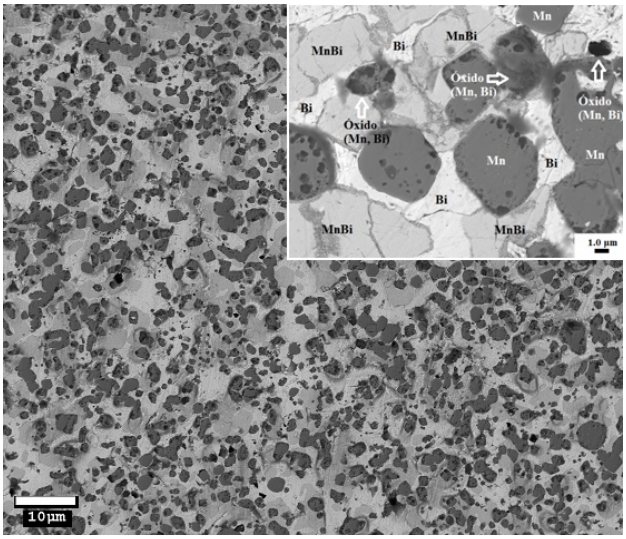

FIGURE 1. SEM micrograph for the as-cast MnBi alloy with a magnification of 1000x. Inset: LTIP-MnBi zones are visible alongside segregated Mn- and Bi-pure phases.

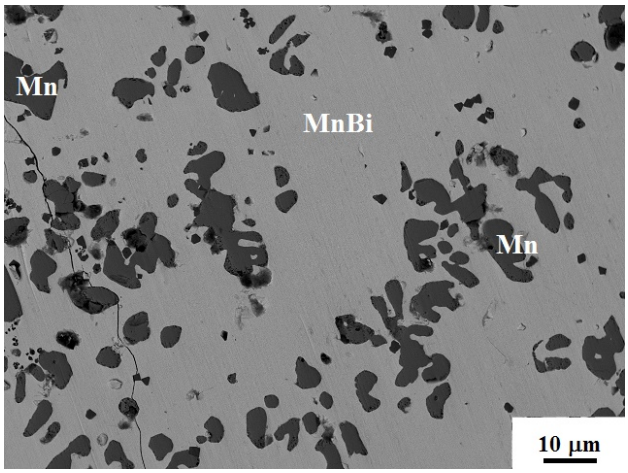

FIGURE 2. SEM micrographs for the annealed MnBi alloy with a magnification of 1000x. LTIP MnBi phase is the predominant phase (gray color). Rounded-like grains (in black) of pure Mn composition with average size of 1.41 μm $\pm$ 0.6 are embedded within the main LTIP matrix.

microstructural details, the MnBi areas exhibit variable sizes, with characteristic lengths between 2.0 and 6.0 microns with no inner inclusions of secondary phases, whereas the Mn and Bi zones display lengths between 5.0 and 3.0 microns, respectively. Few inclusions with darkest contrast within Mn zones correspond to the (Mn,Bi)-oxide. The precipitation of the secondary phases can be explained in terms of the tendency of Bi to nucleate from subcooled liquid before the formation of the peritectic phase LTIP-MnBi [16-21]. On the other hand, segregation of Mn is favored by the presence of Mn-Bi + liquid area during the peritectic reaction.

On the other hand, the microstructure of the annealed alloy displayed in Fig. 2 clearly shows the suppression of pure Bi zones, whereas rounded-like grains of manganese are still present embedded within a majority LTIP-MnBi areas with average length of 1.41 μm $\pm$0.6. Annealing temperature below 613 K promotes the diffusion of more Mn atoms into

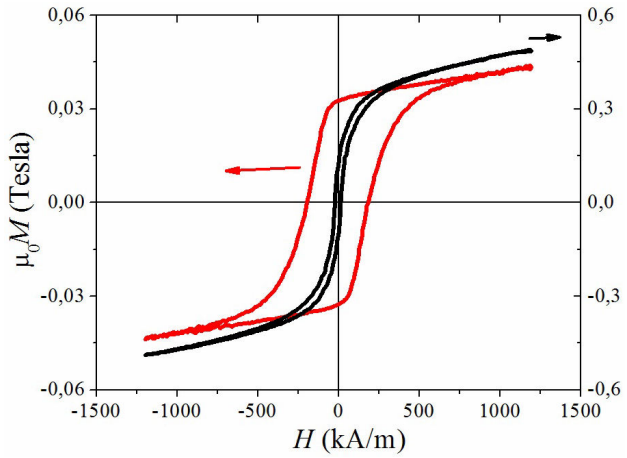

FIGURE 3. Hysteresis curve for the as-cast MnBi alloy (in red, left hand side scale) and the annealed alloy (in black, right hand side scale).

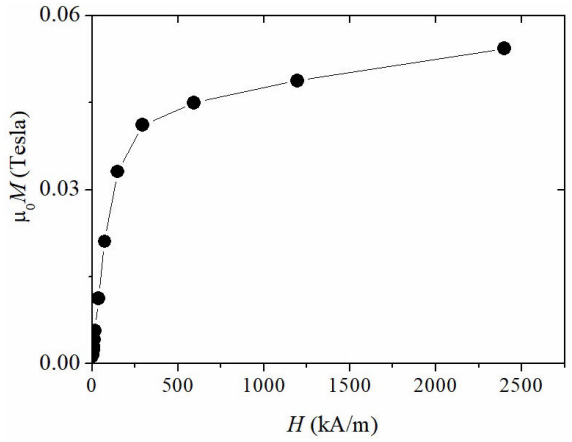

FIGURE 4. Initial magnetization curve for the as-cast MnBi alloy.

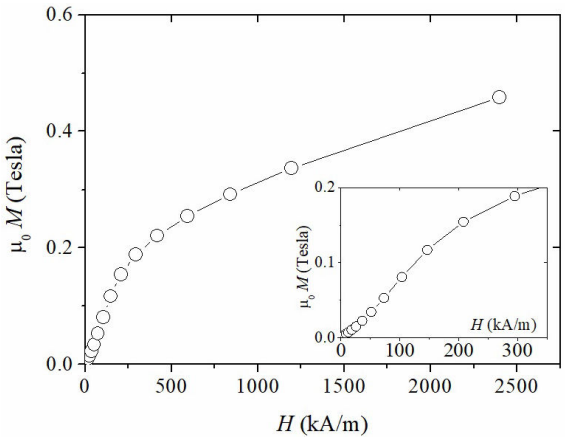

FIGURE 5. Initial magnetization curve for the annealed MnBi alloy. Inset: amplification of the onset of the curve showing lower magnetic susceptibility, relative to as-cast alloys.

bismuth lattice sites and hence, the formation of MnBi phase [22]. Such MnBi areas exhibited a noticeable growth, with uniformly distributed lengths ranging from 30 to 50 microns, as observed in Fig. 4. Some few (Bi, Mn)-oxide areas were also identified. Concerning magnetic properties, hysteresis curves measured at room temperature for the as-cast and annealed alloys are shown in Fig. 3. The as-cast alloy exhibited hard magnetic properties characterized by an H_c of 238 kA/m and $\mu_0 M_s$ of 0.04 T. The presence of non-magnetic Bi-rich zones interspersed between the magnetic MnBi phase causes a dilution effect on the magnetic moment of the alloy, causing the rather low $\mu_0 M_s$. After annealing, a marked decrease for H_c (down to 16 kA/m), alongside an enhancement of $\mu_0 M_s$ (up to 0.47 T) were observed. The increment of $\mu_0 M_s$ can be associated to the significant rise of the volume fraction of ferromagnetic LTIP, as indicated by SEM results already presented.

Within the frame of the nucleation-controlled mechanism for coercivity, for the as-cast MnBi alloy the onset of magnetization occurs at the interface between magnetic LTIP phase and non-magnetic Bi surrounding areas since at such interfaces, the reduction of the magnetocrystalline constant K_1 facilitates the nucleation of reversed domains. The Kronmüller equation, stated previously as Eq. 1, has been used to explain coercivity of an ample diversity of materials obtained by very different techniques, such as Ba-hexaferrites [23], nanosized polycrystalline Nd-Fe-B, Sm-Co, Sm-Fe-Ga-C and Sm-Fe-N alloys [13] and even for similar polycrystalline MnBi alloys obtained by powder metallurgy technique [24]. Since both α_K, N_{eff} parameters are not temperature dependent, it is feasible to use them as fitting factors in Eq. 1. Taking into account that the reported variation of α_K, N_{eff} parameters for hard magnetic alloys with similar microstructural characteristics lies between 0.89 -0.93 and 1.0 -5.0, respectively [25], we use $\alpha_K = 0.90$ and $N_{\text{eff}} = 1.5$ to obtain $H_c = 238$ kA/m, which coincides with the experimental coercivity. This result suggests the nucleation controlled mechanism as the origin of coercivity for our as-cast MnBi alloy. In addition, the initial magnetization curve for this same alloy is displayed in Fig. 4, for which the steep slope at the onset of the curve, associated to the initial magnetic susceptibility, strongly suggests easy displacement of domain walls within the magnetic LTIP zones due to the absence of pining centers, such as described in Fig. 1 for the microstructure of the MnBi as-cast alloy. This feature gives further support to the nucleation of reverse domains (after saturation) as the coercivity mechanism for this alloy.

For the annealed alloy, the significant variation of magnetic properties is indicative of a switching of coercivity mechanism causing a magnetic softening of the alloy. Specifically, the reduction of H_c can be ascribed to the formation of extensive areas of ferromagnetic LTIP (of up to 50 microns, see Fig. 2), favoring the formation of magnetic domain walls, which in turn, switches the coercivity mechanism from nucleation to pinning process, and hence, to lower Hc values. The formation of magnetic domains for structures above 0.86 μm is feasible since the critical length Lcrit given by Eq. (2) for MnBi alloys yields $L_{\text{crit}} = 0.864$ μm (using $A = 2.86 \times 10^{-11}$ J/m [13]). Upon the formation of magnetic domains, the secondary Mn grains (with significantly reduced magnetic properties relative to LTIP-MnBi) act as inclusions to pinning of domain walls. Therefore, the propagation field H_p (and hence, the coercivity field H_c) given by Eq. (3) can be calculated for the MnBi wall energy of $\gamma_w = 4\sqrt{AK_1} = 2.03 \times 10^{-2}$ J/m^2, $\mu_0 M_s = 0.73$ T (for the LTIP phase) and $R_0 = 1.41$ μm (corresponding to the average value of the Mn grains) as $H_p = 19.7$ kA/m, which is very close to the experimental coercivity. Complementary, the initial magnetization curve for this annealed alloy is displayed in Fig. 5, for which the slope at the onset of the curve, associated to the initial magnetic susceptibility, is much less pronounced compared with the as-cast alloy, which reflects the constrained displacement of domain walls due to their pinning at the Mn inclusions described for Fig. 2. This feature gives further support to the pinning of domain walls as the coercivity mechanism for this alloy.

4. Conclusions

The coercivity mechanism of MnBi alloys is strongly dependent on phase constitution and microstructural features. For MnBi alloys obtained by suction casting technique, the modulation of Bi-rich zones surrounding the ferromagnetic LTIP is critical to achieve high coercivity values by means of nucleation controlled reversal mode for LTIP zones not exceeding 6 microns, whereas for extended MnBi over 10 microns, coercivity mechanism switched to pinning of domain walls promoted by the formation Mn-based inclusions embedded within extensive LTIP areas.

Acknowledgments

I. Betancourt acknowledges financial support from research project UNAM-PAPIIT IN103216. J. Zamora is grateful for the scholarship received from UNAM-PAPIIT IN103216 and CONACyT-Mexico.

1. X. Guo, X. Chen, Z. Altounian, and J.O. Strom-Olsen, *Phys. Rev. B* (1992) **46** 14578-14582.
2. T. Chen and W.R. Sturius, *IEEE. Trans. Magn*, **10** (1974) 581-586.
3. H.J. Williams, R.C. Sherwood and O.L. Boothby, *J. Appl. Phys* **28** (1957) 445-447.
4. X. Guo, X. Chen, Z. Altounian and J.O.S. Olsen, *J. Appl. Phys*, **73** (1993) 6275-6277.
5. J. Ping Liu, E. Fullerton, O. Gutfleishch, and J. David *Sellmyer: Nanoscale Magnetic Materials and Applications*, first edition, Springer, US, (2009) 476-479.
6. Yi. Liu, and D.J. Sellmyer, *Shindo: Handbook of Advanced Magnetic Materials* **1** first edition, (Springer, US, 2006). pp. 8, 30, 31.
7. J.M.D. Coey, *IEEE Trans. Magn.* **47** (2011) 4671-4681.
8. H. Okamoto *Bi-Mn phase diagram. Alloy Phase Diagrams* Materials Park. OH: ASM International, (1990) pp 2/102.
9. A.F. Andresen, *Acta. Chem. Scand* **21** (1967) 1543-1554.
10. R. Nithya *et al*., *J. Supercond. Nov. Magn*, **26** (2013) 3161-3165.
11. F. Yin and N. Gu, *J. Mater. Sci. Technol* **12** (1996) 335-341.
12. K. Koyama, T. Onogi, Y. Mitsui, Y. Nakamori, S. Orim, and K. Watanabe, *Mater. Trans* **48** (2007) 2414-2418.
13. H. Kronmüller and M. Fähnle, *Micromagnetism and the microstructure of ferromagnetic solids*, (Cambridge University Press, Cambridge, 2003).
14. H. Kronmüller, *Micromagnetic Background in Hard Magnetic Materials. In Supermagnets, Hard Magnetic Materials*, Eds. G.J.Long, F. Grandjean, Kluwer, (Dordrecht, 1991), p. 461.
15. R. Skomski and J.M.D. Coey, *Permanent Magnetism*, (Institute of Physics, London, 1999), p. 185.
16. T. Saito, R. Nishimura, and D. Nishio-Hamane, *J. Magn. Magn. Mater* **349** (2014) 9-14.
17. D.T. Zhang, S. Cao, M. Yue, W.Q. Liu, J.X. Zhang and Y. Qiang, *J. Appl. Phys* (2011) **109** 07A722.
18. S. Kavita, U. M.R. Seelam, D. Prabhu and R. Gopalan, *J. Magn. Magn. Mater* **377** (2015) 485-489.
19. V. Basso, E.S. Olivetti, L. Martino, and M. Küpferling, *Int. J. Refrig* **37** (2014) 266-272.
20. J.B. Yang *et al*., *J. Phys.: Condens. Matter* **14** (2002) 6509-6519.
21. B. Ciszewski, J. Kozubowski, T. Patej and J. Sadowski, *Memories Scientifique Rev. Metallurg* **LXIX** (1972) 159.
22. W. K. Unger and M. Slotz, *J. Appl. Phys* **42** (1971) 1085-1089.
23. V.T.M.S. Barthem *et al.*, *Physica B* **319** (2002) 127.
24. C. Curcio *et al.*, *Physics Procedia* **75** (2015) 1230
25. X.C. Kou, H. Kronmüller, D. Givord, and M.F. Rossignol, *Phys Rev B* **50** (1994) 3849.